Aerosol Science and Technology

ISSN: 0278-6826 (Print) 1521-7388 (Online) Journal homepage: https://www.tandfonline.com/loi/uast20

Performance Evaluation of the Sampling Head and Annular Kinetic Impactor in the Savannah River Site Alpha Continuous Air Monitor

Bean T. Chen , Mark D. Hoover , George J. Newton , Sandra J. Montaño & Donald S. Gregory

To cite this article: Bean T. Chen , Mark D. Hoover , George J. Newton , Sandra J. Montaño & Donald S. Gregory (1999) Performance Evaluation of the Sampling Head and Annular Kinetic Impactor in the Savannah River Site Alpha Continuous Air Monitor, Aerosol Science and Technology, 31:1, 24-38, DOI: 10.1080/02786829909709774

To link to this article: https://doi.org/10.1080/02786829909709774

Published online: 07 Jan 2010.

Submit your article to this journal

Article views: 187

Citing articles: 5 View citing articles

Full Terms & Conditions of access and use can be found at
https://www.tandfonline.com/action/journalInformation?journalCode=uast20

Aerosol Science and Technology 31:24–38 (1999)
© 1999 American Association for Aerosol Research
Published by Taylor and Francis
0278-6826/99/$12.00 + .00

Performance Evaluation of the Sampling Head and Annular Kinetic Impactor in the Savannah River Site Alpha Continuous Air Monitor

Bean T. Chen, Mark D. Hoover, George J. Newton, Sandra J. Montaño, and Donald S. Gregory
NATIONAL INSTITUTE FOR OCCUPATIONAL SAFETY AND HEALTH, HEALTH EFFECTS LABORATORY DIVISION, 1095 WILLOWDALE RD., MORGANTOWN, WEST VIRGINIA 26505 (B.T.C.), INHALATION TOXICOLOGY LABORATORY, LOVELACE BIOMEDICAL AND ENVIRONMENTAL RESEARCH INSTITUTE, LOVELACE RESPIRATORY RESEARCH INSTITUTE, P. O. BOX 5890, ALBUQUERQUE, NM 87185 (M.D.H., G.J.N., S.J.M.), AND HEALTH PROTECTION DEPARTMENT, WESTINGHOUSE SAVANNAH RIVER COMPANY, AIKEN, SC 29803 (D.S.G.)

ABSTRACT. This paper describes evaluation and testing of the Savannah River Site (SRS) impactor-type alpha continuous air monitor (CAM) to determine the particle delivery and collection efficiency in the device using fluorescence-labeled, polystyrene latex spheres and liquid droplet aerosols. Particle sampling efficiency through the dome-shape sampling inlet for particles with aerodynamic diameters of 6.2 and 10 μm was 98% at 20 cfm (566 L/min), 90% at 32 cfm (906 L/min), and 87% at 40 cfm (1132 L/min) sampling flow rates. Internal delivery efficiency through the CAM was > 94% at 20 and 32 cfm for 0.5-, 1.1-, 2.2-, and 3.2-μm particles and > 90% for 6.2-μm particles. For 10-μm particles, the internal delivery efficiency was 91% at 20 cfm and decreased to 83% at 32 cfm and 77% at 40 cfm. The 50% cutoff aerodynamic diameter for the impactor was 3.2 μm at 20 cfm, 2.6 μm at 32 cfm, and 2.3 μm at 40 cfm. For a typical radioactive aerosol in the workplace (activity median aerodynamic diameter of 5 μm with a geometric standard deviation of 2), these cutoff diameters provide collection efficiencies of 74% at 20 cfm, 83% at 32 cfm, and 87% at 40 cfm. The normal grease layer of 1.5 mg that is routinely applied to the planchet of the SRS CAM was adequate to quantitatively retain all collected particles with diameters of 3.2 μm or less at flow rates of 20, 32, and 40 cfm. For particle sizes of 6.2 and 10 μm, approximately 80–85% of the particles were retained on the impactor planchet and 15–20% were re-entrained into the exhaust airstream due to particle bounce. The delivery and collection efficiencies in the SRS CAM can be combined to give overall efficiencies for detection of airborne actinide aerosols as a function of particle size. For 6.2 and 10 μm aerodynamic diameter particles, the total collection efficiency of the SRS CAM at 20, 32, and 40 cfm exceeds the conservative assumption of 50% efficiency for plutonium particle collection that has been traditionally used at SRS.

INTRODUCTION

Alpha continuous air monitors (CAMs) are used to detect airborne plutonium and other alpha-emitting radionuclides in nuclear facilities. Most alpha CAMs collect airborne particles on a filter that is located in front of a radiation detector and then use alpha spectrometry to separate the radiation emissions of interest from the background interference of naturally occurring, alpha-emitting radon progeny (McFarland et al. 1992). For many years, the Savannah River Site (SRS) has used an innovative, high-volume, annular-type impactor CAM to monitor airborne plutonium in the workplace. In the SRS CAM, airborne plutonium particles are inertially separated from the smaller ambient radon progeny and then collected on a greased zinc sulfide (ZnS)-coated, plastic planchet for subsequent detection and counting of alpha emissions from the particles (Collins 1956; Tait 1956).

The purpose of this study was to confirm the particle sampling and collection efficiency for the SRS CAM. Available results indicated that operation of the CAM at a nominal flow rate of 40 ft^3/min (cfm; 1132 L/min) provided a collection efficiency of approximately 90% for particles > 0.5 μm in geometric diameter (Alexander 1966). Tait (1956) reported that operation of the CAM at 25 cfm (708 L/min) provided a 50% collection efficiency for dust particles with a physical diameter of 0.5 μm and a density of 2.3 g/cm^3 (i.e., a nominal aerodynamic diameter of 0.8 μm). In addition, results from environmental sampling (Hoy 1956) indicated that the collection efficiency was 95% for airborne plutonium particles and 5% for radon progeny. However, these studies did not provide adequate data to document the overall performance of the SRS CAM for particle sizes up to 10 μm aerodynamic diameter at the flow rates of operational interest at SRS (i.e., 20–40 cfm; 566–1132 L/min). This paper provides the overall collection efficiencies of the SRS CAM as a function of particle size and flow rate by combining (1) the particle collection efficiency and particle bounce effect in the impactor, (2) the particle penetration efficiency in the sampling head, and (3) the percent of internal losses in the CAM. This study is part of a comprehensive evaluation of the technical basis for use of the SRS CAM in U.S. Department of Energy facilities.

EXPERIMENTAL

Aerosol Generation

Monodisperse, fluorescence-tagged polystyrene spheres in either aqueous suspension or powder form were used to study the efficiency of the sampling head, separation efficiency of the impactor, and the percent internal loss of particles inside the CAM. Polystyrene latex (PSL) microspheres (Polysciences, Inc., Warrington, PA), with fluorescent dye in yellow-green (excitation maximum = 458 nm, emission maximum = 540 nm) and nominal sizes of 0.46, 1.07, 2.16, and 3.2 μm, were serially generated in a Lovelace nebulizer (In-Tox Products, Albuquerque, NM). Different amounts of ethanol were mixed with the PSL suspensions to produce aerosols of desired concentrations and predominantly single particles by nebulization. Dry, filtered air was then added to evaporate alcohol droplets in the aerosol. For generation of particles > 5 μm, a small-scale powder disperser (TSI, Inc., St. Paul, MN) was used to disperse samples of dry monodisperse polystyrene divinylbenzene (PSDB) spheres (Dukes Scientific, Palo Alto, CA). These monodisperse PSDB particles have fluorescent dye in green (excitation maximum = 459 nm, emission maximum = 512 nm) and nominal aerodynamic diameters of 6.2 and 10 μm.

The generation efficiency of the powder disperser is approximately 50–60% at the flow rate of 18.5 L/min (Chen et al. 1995). For some of the inlet efficiency tests, green dye-tagged PSDB particles with diameters of 6.2 or 10 μm were mixed with ethanol and serially generated with a Lovelace nebulizer as described above. For both types of generation methods, the aerosols of monodisperse particles were passed through a ^{85}Kr source to reach a state of Boltzmann charge equilibrium before being used as test aerosols. An aerodynamic particle sizer (TSI Inc., Model APS33B) was used to monitor the monodispersity of test aerosols.

SRS CAM Configurations

Two configurations of the impactor-type CAM are used at SRS: portable units that operate at a nominal flow rate of 32 cfm (906 L/min) using their own vacuum pumps, and installed units that operate under house vacuum at a nominal flow rate of 40 cfm. During routine operations in the workplace, room air is drawn into the portable CAM through a dome-shaped inlet, or into the installed CAM through an extractive sampling line. Both configurations use identical components for the inlet tube, light-tight sampling chamber, aerosol kinetic impactor, and detector assembly as shown in Figure 1A. Linear velocities and Reynolds numbers for the CAM inlet assembly and kinetic impactor are presented for these flow conditions in Table 1, along with the important dimensions of the sampling inlet and impactor nozzles.

Inside the light-tight housing of the CAM, the airstream passes through the annular kinetic impactor by entering the outer section of the cone and converging to the cylindrical section with an instantaneous increase of air velocity (see the detailed diagram in Figure 1B). As a result, the airborne particles are accelerated at the annular nozzle and are then forced to negotiate a 180° turn at the opening of the nozzle. Particles with large aerodynamic diameters cannot follow the streamline and impact on the collection planchet. Particles with smaller aerodynamic diameters (including nearly all of the ambient radon progeny particles) are able to negotiate the turn and follow the airstream and exhaust through the blower without being sampled. A uniform layer of silicone grease (Dow Corning® No. 200, Midland, MI, with a viscosity of 600,000 centipoise) is manually applied to the collection surface (the concave side shown in Figure 1B) of the planchet to minimize particle bounce. The typical mass of the grease layer used at SRS is 1.5 mg. That mass of grease has generally been considered large enough to retain at least 50% of the particles impacting the collection planchet, while being small enough to avoid excessive attenuation of alpha particle energy in the grease layer.

Evaluation of the Inner Flow Path and Impactor Stage of the SRS CAM

In the first phase of the study, we evaluated the collection efficiency of the impactor and the internal losses in the housing and impactor assembly. During this evaluation, the dome-shaped inlet shroud was removed from the CAM inlet and the CAM was connected directly to the aerosol generation system. The test aerosol was released at the center of the inlet tube and ambient air was added to provide the appropriate total flow to the CAM. We used a standard portable CAM for tests at 20 and 32 cfm, and we added a larger vacuum pump for tests at 40 cfm. The tests at 20 cfm were included to evaluate the ability of the CAM to function at a lower-than-normal flow rate that might inadvertently occur during a routine operation in the workplace.

No exhaust filters are used in the SRS CAM during routine operations. However,

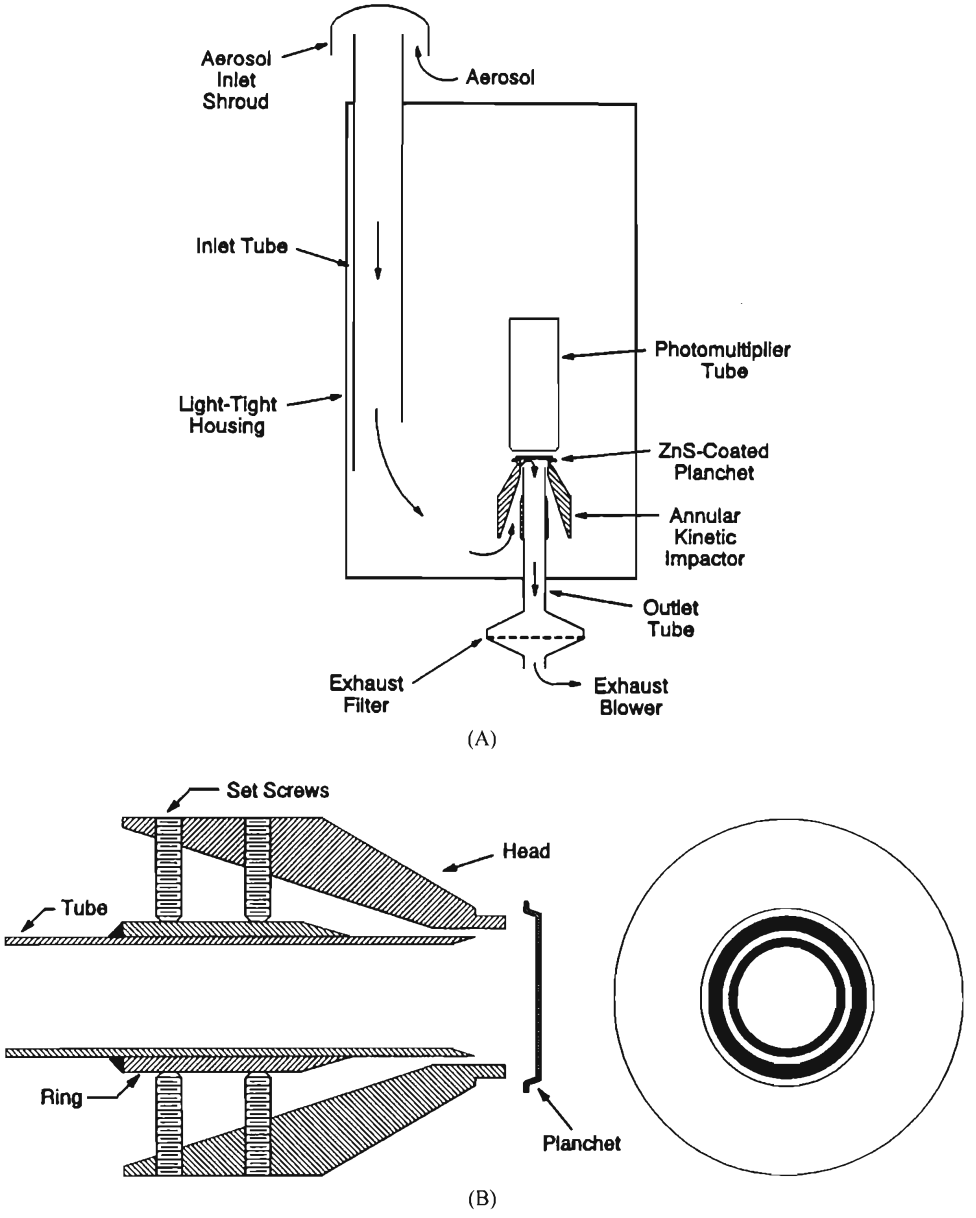

FIGURE 1. Schematic diagrams of (A) the SRS CAM with a backup filter installed for testing purposes to measure particle penetration through the impactor CAM, and (B) a detailed view of the annular-jet impactor. The detailed dimensions of the impactor, e.g., nozzle diameter and throat length, are described in Alexander (1966).

TABLE 1. Operating conditions and flow parameters for the impactor stage and sampling inlet in the SRS CAM.

(A) annular-jet impactor[a]

Sampling Flow Rate (cfm)	Velocity Through the Nozzle (m / sec)	Nozzle Reynolds Number	Mass of Silicone Grease on Planchet (mg)
20	55.7	11,900	15
32	89.2	19,000	1.5
40	111	23,800	1.5

[a]The nozzle width and the nozzle-to-planchet distance of the annular-jet impactor are 1.97 mm and 6.35 mm, respectively.

(B) sampling inlet[b]

Sampling Flow Rate (cfm)	Velocity Through Annular Inlet Nozzle (m / sec)	Inlet Nozzle Reynolds Number[c]
20	1.83	4,050
32	2.92	6,480
40	3.65	8,090

[b]The width of the annular slit between the inlet shroud and the inlet tube is 2.04 cm. The vertical distance from the top of the inlet shroud to the inlet tube is 4.14 cm.

[c]Values for the Reynolds number of the inlet nozzle was determined from $(\rho v/\eta)(4A/P)$, where ρ is the air density, v the mean air velocity, η the air viscosity, A the cross-sectional area of the annular inlet, and P the perimeter of the inlet.

as noted in Figure 1A, we installed a 90-mm diameter backup exhaust filter (Fluoropore 5 μm filter, Millipore Corp., Bedford, MA) between the impactor stage and the vacuum pump to collect particles that were not deposited on the collection planchet.

The Fluoropore filter was selected because of its low pressure drop. The filter is a Teflon membrane bonded to polypropylene high-density fibers. The pressure drop of the filter is exceptionally low because of the open structure of the Teflon microfibrils that make up the collection surface of the filter. These polypropylene fibers provide support for the Teflon membrane, but contribute negligible pressure drop. The Fluoropore 5 μm filter has a collection efficiency of better than 99.99% for particles larger than 1 μm aerodynamic diameter and retains a collection efficiency of $> 98.3\%$ for particles as small as 0.03 μm (Hoover and Newton 1992). The Fluoropore filters used in this study were provided by Millipore Corporation with a black-colored support backing to allow easy identification of the collection side. This version of the filters was developed in conjunction with Millipore Corporation for use in spectrometry-based alpha CAMs (Hoover and Newton 1991 and 1992). The sampling flow rate was measured before and after each test by attaching a calibrated laminar flow element (Model 50MC2-2, Meriam Instrument Company, Cleveland, OH) to the CAM inlet tube. The pressure drop across the flow element was measured with either an inclined manometer (Dwyer Instruments, Inc., Michigan City, IN) or a differential pressure sensor (Model 8360 Velocicalc, TSI, Inc., St. Paul, MN).

Two different masses (1.5 and 15 mg) of silicone grease (Dow Corning® No. 200, Midland, MI) were applied to the planchet to study the effects of surface coating on particle bounce. The smaller mass of 1.5 mg was used in the normal impactor collec-

tion tests because it is the typical grease mass used at SRS. The larger mass of 15 mg was used to determine the impactor efficiency when no particle bounce could occur from the planchet once a particle had made contact with the grease layer. An optical microscope (Olympus, Model BHS, Lake Success, NY) with a BH2-RFC reflected-light fluorescence attachment was used to examine the concentration of fluorescent microspheres on the collection planchets and backup filters for any indications of particle-bounce phenomena.

The collection efficiency tests for fluorescent particles were done with glass planchets in the impactor stage because we found that ethyl acetate (the organic solvent used to extract fluorescent dye from the PSL and PSDB particles) also dissolved the normal ZnS(Ag)-coated, plastic planchets. The presence of dissolved ZnS and plastic residues in the test solutions interfered with proper measurements of fluorescence from the dye particles. Ethyl acetate also damaged the black-painted surfaces inside the light-tight housing assembly. Therefore, a removable Teflon sheet was used in the bottom of the light-tight housing to assess particle deposition on the horizontal surface under the inlet tube. The area below the inlet tube was the only surface in the light-tight housing assembly that appeared to accumulate particles. Quantitative removal of the fluorescent dye from the steel and brass surfaces of the inlet tube, impactor cone, and outlet tube was not a problem.

After each experiment, the CAM was disassembled and various internal parts, including the inlet tube, Teflon sheet (bottom surface of the housing), impactor cone, glass planchet, brass tube, and backup filter, were taken out and rinsed with ethyl acetate. The filter was immersed in ethyl acetate and then subjected to ultrasonic agitation for 5 min. This procedure was then repeated to ensure that more than 95% of the fluorescence was extracted from each disassembled part or filter. Samples were then analyzed using a fluorescence spectrophotometer (Hitachi, Model F-1200, Danbury, CT). The excitation and emission wavelengths were set for maximum fluorescence detection with a minimum noise-to-signal ratio.

A complete evaluation of internal particle collection efficiency was done at a 20 cfm flow rate for all particle sizes with a "no-bounce" grease layer of 15 mg. A similar evaluation was also done at 32 cfm with a normal grease layer of 1.5 mg. Those tests were conducted to investigate the relative importance of particle bounce and particle losses in the CAM as well as the mathematical relationship for the effective cutoff diameter of the impactor stage as a function of flow rate. Because internal particle losses were found to be quite small at flow rates of 20 and 32 cfm for all particle sizes smaller than 6.2 μm aerodynamic diameter, the internal efficiency tests at 40 cfm were only done for particles with aerodynamic diameters of 6.2 μm and 10 μm. Detailed flow conditions are presented in Table 1A.

Evaluation of Particle Delivery and Losses in the Sampling Inlet

The second phase of the study was designed to evaluate the particle sampling efficiency of the dome-shaped aerosol inlet assembly of the SRS CAM (Figure 1A). This was done by removing the inlet shroud and inlet tube assembly (Figure 2B) from the CAM and testing it in a 1.8 m^3 vertical-flow aerosol test chamber that is similar to the test system of Marple and Rubow (1983; Figure 2A). Each test aerosol was introduced at the top of the chamber through an opposing, dilution air jet that created turbulence to mix the aerosol. The uniformity of aerosol distribution was further improved by placing a 10-inch box fan

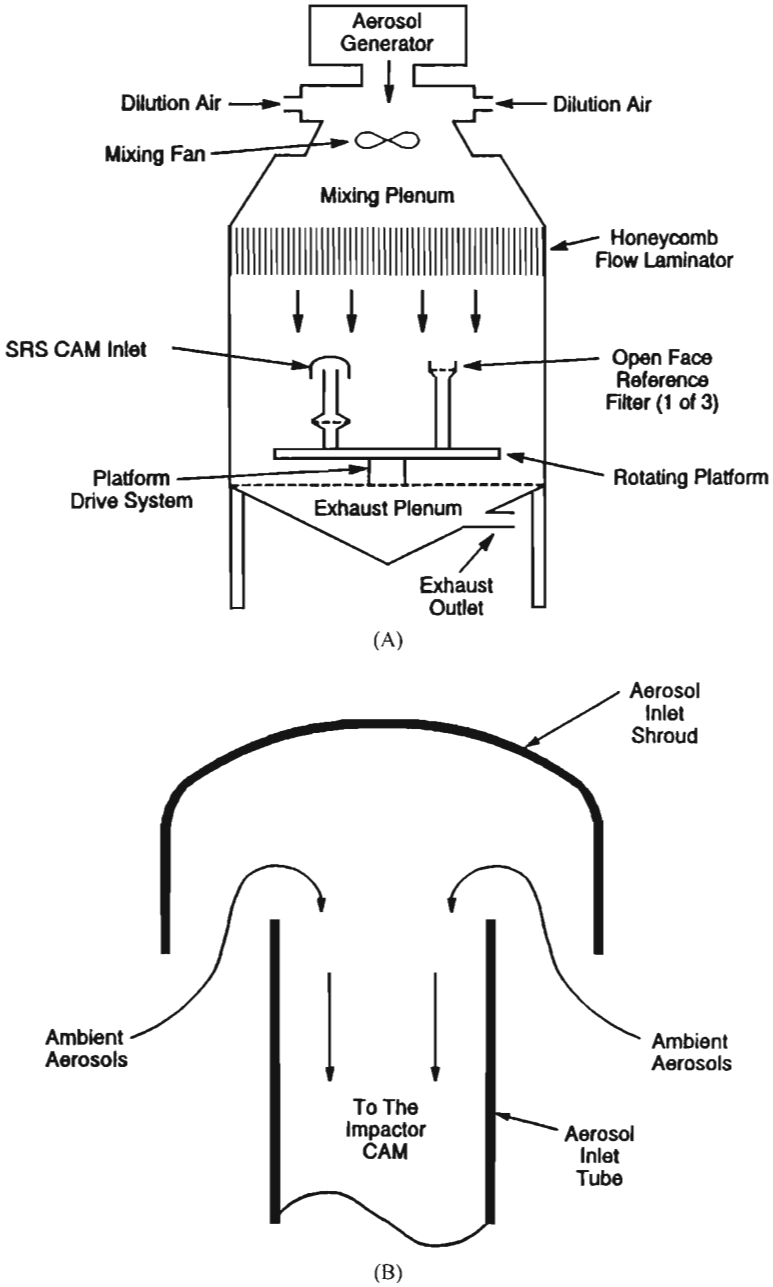

FIGURE 2. Schematic diagrams of (A) the vertical aerosol wind tunnel configuration for testing the inlet efficiency of the SRS CAM and (B) a detailed view of the SRS CAM sampling head.

in the mixing plenum at the top of the chamber. This was followed by a 10-cm-thick honeycomb structure that was inserted above the test section of the chamber to reduce eddy currents and thereby present the sampling area with a well-defined, downward airflow. To ensure that spatial variations of concentration and size distribution were minimized in the test chamber, the CAM inlet section (along with three, 47-mm, Fluoropore reference filter samplers) was placed on a 76-cm platform rotating at 1 rpm. The CAM inlet was connected to a 90-mm diameter, Fluoropore backup filter identical to the arrangement used to test the internal collection efficiency of the CAM. The flow rates through the inlet head were 20, 32, and 40 cfm (Table 1B), and the total flow rate through the chamber was between 70 cfm and 140 cfm. Each of the three, 47-mm-diameter, Fluoropore 5 μm reference filters was operated at a flow rate of 1 cfm to determine the mean aerosol concentration in the chamber.

After each experiment, the inlet shroud, delivery tube, backup filter, and three reference filters were disassembled. The internal and external surfaces of the shroud and tube were separately rinsed with ethyl acetate to extract fluorescent dye from the deposited particles. The filters were separately immersed in ethyl acetate, then analyzed as described above.

The inlet efficiency tests began with a particle aerodynamic size of 10 μm and continued with a particle aerodynamic size of 6.2 μm. Results from those tests indicated that the inlet efficiency for smaller particle sizes would approach 100% and would not merit additional measurement.

Data Analysis

The impactor efficiency and internal loss factors were determined by a calculation involving the fluorescent intensities of the samples collected from the inlet tube, Teflon sheet (bottom surface of the housing), impactor cone, glass planchet, brass tube, and backup filter. For particles of a given size, the separation efficiency ($\eta_{impactor}$) of the impactor was computed from

$$\eta_{impactor} = \frac{F_{gp}}{F_{gp} + F_{bt} + F_{bf}}, \tag{1}$$

where F_{gp}, F_{bt}, and F_{bf} represent the fluorescent intensities of the particles deposited on the surfaces of glass planchet, brass tube, and backup filter, respectively (Figure 1), and the sum of the values in the denominator represents the fluorescent intensities of the particles that passed through the impactor. Wall loss, *WL*, on the internal surface of the CAM (excluding the inlet shroud) was computed from

$$WL = \frac{F_{ts} + F_{ic} + F_{bt}}{F_{ts} + F_{ic} + F_{gp} + F_{bt} + F_{bf}}, \tag{2}$$

where F_{ts} and F_{ic} represent the fluorescent intensities of the particles deposited on the surfaces of the Teflon sheet and impactor cone, respectively (Figure 1A). The sum of the values in the denominator represents the fluorescent intensities of the particles that passed through the internal housing of the CAM. Other surfaces inside the CAM housing had $< 1\%$ of the total fluorescence deposited in the CAM and were not included in the analysis. Although deposits on the inlet tube were analyzed in this part of the study at all flow rates and particle sizes, the fluorescent intensities in the samples were not detectable and not included in Equation (2). This was expected because, without the inlet shroud in the flow path, the test aerosols entered the center of the inlet tube and had a high ratio of ambient sheath air to surround the particles and prevent particle losses inside the tube. Nevertheless, particle deposits in the inlet tube

were included in the analysis below as part of the evaluation for the sampling inlet.

For determining sampling efficiencies and internal losses of the sampling inlet, the fluorescent intensities of the samples collected from the 90-mm backup filter, the three 47-mm reference filters, the inlet shroud, and the inlet tube were used in the calculation. For particles of a given size, the efficiency (η_{inlet}) was computed from

$$\eta_{inlet} = \frac{3FI_{bf}}{Q_{bf}\left[\frac{FI_{f1}}{Q_{f1}} + \frac{FI_{f2}}{Q_{f2}} + \frac{FI_{f3}}{Q_{f3}}\right]}, \quad (3)$$

where FI_{bf}, FI_{f1}, FI_{f2}, and FI_{f3} represent the fluorescent intensities of the particles deposited on the backup filter and 3 reference filters, respectively (Figure 2A), and Q_{bf}, Q_{f1}, Q_{f2}, and Q_{f3} were the flow rates through the sampling inlet and 3 reference filters, respectively. Wall loss at the inlet shroud and inlet tube, *WLI*, was computed from

$$WLI = \frac{FI_{is} + FI_{es} + FI_{it} + FI_{et}}{FI_{is} + FI_{es} + FI_{it} + FI_{et} + FI_{bf}}, \quad (4)$$

where FI_{is}, FI_{es}, FI_{it}, FI_{et}, and FI_{bf} represent the fluorescent intensities of the particles deposited on the internal and external surfaces of the inlet shroud and inlet tube, respectively (Figure 2B). The sum of the values in the denominator represents the fluorescent intensities of particles that passed through the sampling inlet.

RESULTS

Separation Efficiency of the Impactor

Table 2 shows the percentage of fluorescent intensity in particles deposited at four different sections of the SRS CAM at a flow rate of 20 cfm with a grease mass of 15 mg (the no bounce condition). The inlet section includes the bottom surface (Teflon sheet) and the internal surface of the impactor cone; the glass planchet is where particles are normally collected for alpha radioactivity counting; the outlet section represents the internal surfaces of the connector tubing between the planchet and the backup filter; and the backup filter collects any particles exiting the impactor. Particle separation efficiency on the planchet increased with particle size, with a 50% cutoff aerodynamic diameter of approximately 3.2 μm. Figure 3 relates these separation efficiency results (Equation (1)) to a dimensionless particle diameter, the square root

TABLE 2. Percentage of fluorescence content on the inlet section, planchet, outlet section, and backup filter of the SRS impactor CAM. Sampling flow rate was 20 cfm with a 15-mg grease layer on the collection planchet. Each reported value is the mean value obtained from three experiments.

Deposition Surface		Aerodynamic Diameter of Polystyrene Latex and Polystyrene Divinylbenzene Particles (μm)					
		0.5	1.1	2.2	3.2	6.2[a]	10[a]
Inlet Section	Bottom Surface	0	0	0.3	0	3.3	7.6
	Impactor Cone	0	0.8	1.5	0.8	2.0	1.2
Planchet	Glass Planchet	0.4	10.1	33.6	46.6	88.2	88.2
Outlet Section	Connector Tubing	0	0.9	4.5	1.1	0	0.2
Filter	Filter	99.6	88.1	60.1	51.5	6.5	2.8
Wall Loss[b]		0	1.7	6.3	1.9	5.3	9.0

[a] These aerosols were generated from dry powders; others were generated from liquid suspensions.
[b] Wall loss was determined based on Equation (2).

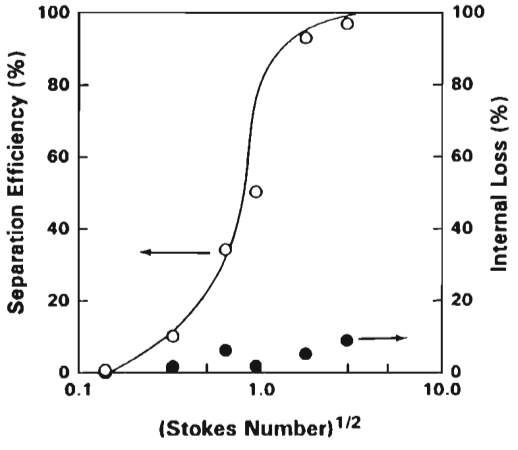

FIGURE 3. Particle separation efficiency and internal wall loss of the SRS CAM as a function of the square root of the dimensionless Stokes number at a total flow rate of 20 cfm with a grease mass of 15 mg on the collection planchet. Open circles represent the separation efficiency of the annular kinetic impactor and closed circles represent the internal wall losses in the sampling chamber and kinetic impactor.

of Stokes number (Stk), which is defined as

$$Stk = \frac{D_{AE}^2 C V_o}{9\eta W}, \tag{5}$$

where D_{AE} is the aerodynamic diameter, C is the particle slip correction, V_o is the mean fluid velocity at the nozzle throat, η is the air viscosity, and W is a characteristic dimension of the impactor nozzle. (In the case of a conventional impactor, W is the nozzle diameter for a circular jet or = the nozzle width for a conventional rectangular jet where the flow exits on both sides of the jet; in this case, however, W is 2 times the nozzle width for the annular-jet impactor where the flow can only exit on the inner side of the jet.) The $(Stk)^{1/2}$ value corresponding to 50% separation efficiency is approximately 0.98 at the flow rate of 20 cfm and grease mass of 15 mg. This 50%

TABLE 3. Percentage of fluorescence content on the inlet section, planchet, outlet section, and backup filter of the SRS impactor CAM. Sampling flow rate was 32 cfm with a 1.5-mg grease layer on the collection planchet. Each reported value is the mean value obtained from 3 experiments. Values in parentheses for the 6.2-μm and 10-μm aerodynamic particle sizes are from tests at 40 cfm with a 1.5-mg grease layer.

Deposition Surface		Aerodynamic Diameter of Polystyrene Latex and Polystyrene Divinylbenzene Particles (μm)					
		0.5	1.1	2.2	3.2	6.2[a]	10[a]
Inlet Section	Bottom Surface	0.5	1.1	1.0	0.6	7.7 (9.6)	13.4 (20.7)
	Impactor Cone	0.3	1.0	0.8	0.9	0.9 (1.6)	0.7 (1.0)
Planchet	Glass Planchet	5.0	15.3	37.7	47.6	69.8 (68.9)	70.4 (60.8)
Outlet Section	Connector Tubing	0.9	3.3	2.4	2.1	0.4 (1.8)	2.9 (1.5)
Filter	Filter	93.3	79.2	58.1	48.8	21.1 (18.0)	12.7 (14.7)
Wall Loss[b]		1.7	5.4	4.2	3.6	9.0 (13.0)	17.0 (23.2)

[a] These aerosols were generated from dry powders; others were generated from liquid suspensions.
[b] Wall loss was determined based on Equation (2).

cutoff $(Stk)^{1/2}$ was used to predict the 50% cutoff aerodynamic diameters at different flow rates. The cutoff diameters at flow rates of 32 and 40 cfm were estimated to be 2.6 and 2.3 μm, respectively. The validity of this prediction was confirmed by conducting a similar test for all particle sizes at 32 cfm with 1.5 mg grease and for particle diameters of 6.2 μm and 10 μm at 40 cfm (see Table 3).

Particle Bounce in the Impactor

Assuming that without any particle bounce the data which relate separation efficiency to $(Stk)^{1/2}$ can be represented by the same dimensionless relationship (Chen et al. 1985), the dimensionless efficiency curve in Figure 3 can be transformed to a dimensioned efficiency curve at a flow rate of interest. This is illustrated in Figure 4, in which the dimensionless data from Figure 3 are plotted as a function of particle size for a flow rate of 32 cfm. Figure 4 also includes the actual particle separation efficiency results that were obtained with 1.5 mg grease on the planchet. At a flow rate of 32 cfm, the empirical data for particle collection efficiency and the predicted value for particle collection efficiency are very close for particles < 3.2 μm aerodynamic diameter. This confirms that the application of 1.5 mg grease mass was sufficient for particles to stick to the planchet once they were deposited. However, the decreased collection efficiencies for particles of 6.2 and 10 μm (compared to the predicted curve) suggest that particle bounce and re-entrainment occurred for the particles > 3 μm. Based on Figure 4, approximately 15–20% of 6.2-μm and 10-μm particles were bounced from the planchets at the flow rate of 32 cfm. Similar results were found for 6.2-μm and 10-μm diameter particles at 40 cfm using a 1.5-mg layer of grease (Table 3). As expected, the decreases in the particle collection efficiency at 40 cfm were slightly greater than those observed at 32 cfm, possibly because of greater particle bounce at the higher impaction velocity. The findings that more particle bounce occurred for larger particles at a greater flow rate agree with those reported in the literature (Hinds 1982). Observations using the fluorescence microscope confirmed that the relative numbers of 6.2-μm and 10-μm particles were much greater on backup filters for the tests involving 1.5-mg grease layers than in the tests involving 15-mg grease layers.

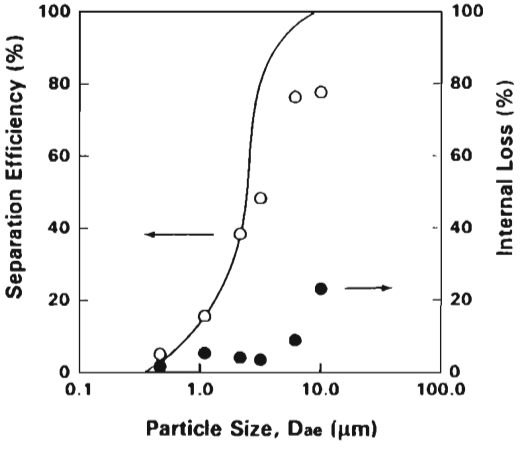

FIGURE 4. Particle separation efficiency and internal wall loss of the SRS CAM as a function of particle aerodynamic diameter at the typical operating flow rate of 32 cfm for the portable version of the SRS CAM. The solid curve is taken from the empirical collection efficiency data presented in Figure 3 to represent the ideal particle collection efficiency that would have occurred when no particle bounce from the planchet. Data were obtained with a grease mass of 1.5 mg on the planchet. Open circles represent the separation efficiency, and closed circles represent the wall losses.

Wall Losses in the CAM

Figures 3 and 4 show the wall losses in the SRS CAM based on fluorescence content reported in Tables 2 and 3 at different flow rates and particle sizes. The percentage of

TABLE 4. Penetration efficiencies and internal losses (values in the parentheses) in the inlet section of the SRS CAM as a function of particle aerodynamic diameter. The aerosols of Polystyrene Divinylbenzene (PSDB) particle were generated from either liquid suspensions or dry powders. Each value is the mean obtained from either two or three experiments.

Flow Rate Through the Sampling Head	Aerodynamic Diameter of the PSDB Particles	
	6.2 μm	10 μm
20 cfm	.98 (.013)	.98 (.016)
32 cfm	.90 (.014)	.91 (.017)
40 cfm	.87 (.031)	.88 (.022)

fluorescence from PSL particles on the bottom surface of the inlet section increased with particle size. That indicates that larger particles had more difficulty negotiating the deflection of flow streamlines and, as a result, were more susceptible to impaction and collection on the bottom surface of the CAM. However, wall losses in the CAM were $< 7\%$ for particles smaller than 6.2 μm, and the losses did not seem to depend on particle size. For 6.2- and 10-μm particles, however, the losses increased with increasing flow rate from about 5–9% at 20 cfm to 9–17% at 32 cfm and to 13–23% at 40 cfm, indicating that the wall loss could be a function of flow rate.

Efficiency and Loss in the Sampling Inlet

Table 4 shows the particle sampling efficiency and wall loss in the dome-shaped inlet shroud and the stainless-steel delivery tube connected to the CAM housing chamber. The efficiency through the sampling inlet was $> 90\%$ for 6.2- and 10-μm diameter particles at 20 and 32 cfm and slightly less for particles at 40 cfm. The efficiency should increase for smaller particles because they would follow flow streamlines better. The wall losses in the sampling inlet were $< 4\%$, with the most noticeable losses occurring on the inner wall of the delivery tube just below the inlet shroud. No other preferential locations for particle accumulation were observed on the internal and external surfaces of the inlet shroud and delivery tube.

DISCUSSION

Particle sampling efficiency through the inlet assembly (shroud and tube) of the CAM was $> 87\%$ for 6.2-μm and 10-μm aerodynamic diameter particles at 40 cfm and increased for smaller flow rates. The internal loss at the sampling inlet was smaller than 4%. Because smaller particles tend to follow streamlines more closely, particles smaller than 6.2 μm were expected to have higher efficiency and smaller loss. Internal delivery efficiencies through the CAM were $> 94\%$ at 20 and 32 cfm for aerodynamic particle sizes of 0.5, 1.1, 2.2, and 3.2 μm and $> 90\%$ for particle sizes of 6.2 μm. For 10 μm particles, the internal delivery efficiency was 91% at 20 cfm and decreased to 83% and 77% at 32 and 40 cfm, respectively. The 50% cutoff aerodynamic diameter for the annular kinetic impactor was 3.2 μm at 20 cfm, which corresponds to values of 2.6 μm at 32 cfm and 2.3 μm at 40 cfm.

Overall, results obtained from the study indicate that the SRS CAM performs well with small wall losses using solid, spherical particles. Although workplace aerosol particles such as the actinide particles are typically not spherical, the sampling and impaction efficiencies for compact particles depends on the aerodynamic behavior of particles in following air streamlines. Generally, the losses are associated with flow rate and particle aerodynamic diameter.

For a typical radioactive aerosol in the workplace with an activity median aerodynamic diameter of 5 μm with a geometric standard deviation of 2 (Dorrian and Bailey 1995; ICRP 1994), these cutoff diameters

provide collection efficiencies of 74% at 20 cfm, 83% at 32 cfm, and 87% at 40 cfm. The phenomenon of particle bounce off the impactor planchet was investigated under the assumption that no particle bounce occurred when the 15-mg grease was applied. Results from fluorescence measurements and microscopic observations of particles collected on backup filters indicated that some bounce of large particles occurs when a 1.5-mg grease layer is used. When using particle sizes of 6.2 and 10 μm, approximately 80–85% of the particles entering the impactor were retained on the collection planchet and 15–20% re-entrained into airstream due to particle bounce. Some particle bounce may also occur at high particle concentrations because of particle-to-particle contact on the thin annular ring of particle collection on the planchet. It was shown that a thick layer of grease, such as 15 mg mass, can reduce particle bounce to a negligible effect, but use of layers thicker than 1.5 mg do not appear necessary to provide reasonable particle collection performance in the CAM. In addition, it is highly desirable to use a relatively modest grease layer thickness such as 1.5 mg mass so that any attenuation to alpha particles emitted from collected actinides will be minimized and radiation counting efficiency will be maximized.

It is useful to compare the results of this study with the historical reports of Tait (1956) and Alexander (1966). Tait (1956) reported that when the device was operated at 25 cfm, it had a 50% collection efficiency for 0.5-μm (physical diameter based on microscopic observation) dust particles with a 2.3 g/cm^3 density. That particle size and density corresponds to a nominal aerodynamic diameter of 0.8 μm. Our results show that the collection efficiency for that particle size is only about 10%, rather than 50%, and that the aerodynamic diameter for 50% collection efficiency at 25 cfm flow rate is actually 2.9 μm (based on the dimensionless Stokes correlation in Equation (5)). Alexander (1966) also reported a smaller effective cutoff diameter than found in our study. Alexander reported that when the device was operated at its nominal flow rate of 40 cfm, it had a collection efficiency of approximately 90% for particles > 0.5 μm in geometric diameter. Our results show a collection of efficiency on the order of 5% for those conditions. Depending on the chemical composition of these 0.5-μm particles, their corresponding aerodynamic diameters could be 1.1 μm for plutonium dioxide particles or 1.9 μm for plutonium metal particles. The reasons for the differences in cutoff size and particle collection efficiency between this study and the studies by Tait (1956) and Alexander (1966) are difficult to pinpoint, mainly because little information was provided by these historic reports. However, it is conceivable that particle types (particle density, shape, and dispersity), sampling methods (inertial impaction vs. filtration), measuring techniques (microscopic counting vs. gravimetric weighing), and expression terminologies (mass median aerodynamic diameter vs. count mean projected area diameter) could contribute to the differences. Nevertheless, the basic performance concepts reported by Tait (1956) and Alexander (1966) for inertial separation of small radon progeny aerosols from larger particles of concern in the workplace is correct.

As noted above, the efficiencies for all aspects of aerosol sampling obtained in our study can be combined to give overall efficiencies for detection of airborne actinides as a function of particle size (Table 5). For 10-μm aerodynamic diameter particles, the total collection efficiency of the SRS CAM was 85% ((0.98 sampling efficiency at the inlet) $\times$ (0.98 delivery efficiency at the inlet) $\times$ (0.88 impactor retention efficiency) = 0.85) at 20 cfm, 62% at 32 cfm, and 51% at

TABLE 5. Illustrations of the combined, overall efficiencies for collection of particle sizes of 0.5, 6.2, and 10 μm aerodynamic diameter on the impactor planchet in the SRS CAM. The combined efficiency calculation is based on internal delivery and collection efficiency values from Tables 2 and 3 and sampling inlet efficiency values from Table 4.

(A) 20 cfm			
Aerodynamic Diameter of Particles (μm)	0.5	6.2	10
Sampling Efficiency at the Inlet (%)[a]	100	98	98
Delivery Efficiency at the Inlet (%)[b]	100	98	98
Retention Efficiency on the Impactor (%)[c]	0.4	88	88
Overall Efficiency (%)	0.4	85	85
(B) 32 cfm			
Aerodynamic Diameter of Particles (μm)	0.5	6.2	10
Sampling Inlet Efficiency (%)[a]	100	90	91
Delivery Efficiency at the Inlet (%)[b]	100	98	98
Retention Efficiency on the Impactor (%)[c]	5	70	70
Overall Efficiency (%)	5	62	62
(C) 40 cfm			
Aerodynamic Diameter of Particles (μm)	0.5[d]	6.2	10
Sampling Inlet Efficiency (%)[a]	~ 100	87	88
Delivery Efficiency at the Inlet (%)[b]	~ 100	97	97
Retention Efficiency on the Impactor (%)[c]	~ 5	69	61
Overall Efficiency (%)	~ 5	58	51

[a] Values are based on the penetration efficiencies presented in Table 4.
[b] Values are calculated from the internal losses listed in Table 4.
[c] Retention efficiency is the percent of particles that enter the sampling inlet retained on the impactor planchet (values obtained from Table 3). For a flow rate of 20 cfm, it is based on the assumption of no particle bounce. For 32 and 40 cfm, however, it considers CAM internal delivery efficiency, impactor collection efficiency, and particle-bounce effect.
[d] Values for 0.5 μm are assumed to be the same as those at 32 cfm.

40 cfm. On the other hand, particles associated with naturally occurring radon progeny are primarily smaller than 0.5 μm. The overall efficiency for these particles is < 5% (Table 5), mainly because of the collection efficiency on the impactor. This indicates that the annular kinetic impactor does bypass the majority of the fine particles to minimize background detection of naturally occurring, alpha-emitting radon progeny. The overall efficiencies for 6.2-μm particles were similar than those for 10 μm, except for the higher value (58%) at 40 cfm. These values for overall system efficiency compared very favorably with the conservative assumption of 50% efficiency of plutonium collection traditionally used at SRS. Therefore, no deviation is recommended from the current assumption used at SRS for the kinetic impactor alpha CAM.

This paper was prepared under funding provided by Order Number AA71928V from Westinghouse Savannah River Company to the Lovelace Biomedical and Environmental Research Institute through U.S. Department of Energy Contract number DE-AC04-76EV01013. Donald S. Gregory was the WSRC project officer for this work. We thank Terese Henson, Bobby Smith, Dan Ratchford, Steve Epperson, Steve Thomas, and Greg Tunno of WSRC for their help and encouragement. We thank Marybeth Marcinkovich, Alice Fencl, Dennis Yazzie, Tony Stephens, and Terry Zimmerman of the Lovelace aerosol science group for their help with the test program. Sandra Montaño of the University of New Mexico participated in this work as a summer research participant under the auspices of the Associated Western Universities. The author BTC is indebted to his NIOSH colleagues for technical review and suggestions and to Drs. Sid Soderholm and Al Munson for encouragement and support.

References

Alexander, J. M. (1966). A Continuous Monitor for Prompt Detection of Airborne Plutonium, *Health Physics* 12:553–556.

Chen, B. T., Yeh, H. C., and Cheng, Y. S. (1985). A Novel Virtual Impactor: Calibration and Use, *J. Aerosol Sci.* 16:343–354.

Chen, B. T., Yeh, H. C., and Fan, B. J. (1995). Evaluation of the TSI Small-Scale Powder Disperser, *J. Aerosol Sci.* 26:1303–1313.

Collins, D. C. (1956). *A Continuous Monitor for Airborne Plutonium*, U.S. AEC Report DP-188, Savannah River Plant, E. I. du Pont de Nemours and Company, Aiken, SC.

Dorrian, M. D., and Bailey, M. R. (1995). Particle Size Distributions of Radioactive Aerosols Measured in Workplaces, *Radiation Protection Dosimetry*, 60:119–133.

Hinds, W. C. (1982). *Aerosol Technology*, John Wiley and Sons, New York, pp. 127–132.

Hoover, M. D., and Newton, G. J. (1991). *Technical Basis for Selection and Use of Filter Media in Continuous Air Monitors for Alpha-Emitting Radionuclides*, ITRI Annual Report 1990-1991, National Technical Information Service, Springfield, VA, pp. 16–19.

Hoover, M. D., and Newton, G. J. (1992). *Update on Selection and Use of Filter Media in Continuous Air Monitors for Alpha-Emitting Radionuclides*, ITRI Annual Report 1991-1992, National Technical Information Service, Springfield, VA, pp. 5–7.

Hoy, J. E. (1956). *Annular Kinetic Impactor*, DPSPU 56-11-30, Savannah River Plant, E. I. du Pont de Nemours and Company, Aiken, SC.

International Council on Radiation Protection (1994). *Human Respiratory Tract Model for Radiological Protection: A Report of a Task Group of the International Commission on Radiological Protection*, ICRP Publication 66, Annals of the ICRP, Vol 24, No. 1–3, Pergamon, Oxford.

Marple, V. A., and Rubow, K. L. (1983). An Aerosol Chamber for Instrument Evaluation and Calibration, Am. Ind. Hyg. Assoc. 44:361–367.

McFarland, A. R., Rodgers, J. C., Ortiz, C. A., and Moore, M. E. (1992). A Continuous Sampler with Background Suppression for Monitoring Alpha-Emitting Aerosol Particles, *Health Physics* 62:400–406.

Tait, G. W. C. (1956). Determining Concentration of Airborne Plutonium Dust, *Nucleonics*, 14:53–55.

Received 25 March 1998; accepted 25 January 1999.